Phys Chem Minerals (2002) 29: 307–318
DOI 10.1007/s00269-001-0237-z

ORIGINAL PAPER

G. V. Gibbs · D. F. Cox · T. D. Crawford
M. B. Boisen Jr · M. Lim

A mapping of the electron localization function for the silica polymorphs: evidence for domains of electron pairs and sites of potential electrophilic attack

Received: 13 August 2001 / Accepted: 11 December 2001

Abstract The electron localization function, η, evaluated for first-principles geometry optimized model structures generated for quartz and coesite, reveals that the oxide anions are coordinated by two hemispherically shaped η-isosurfaces located along each of the SiO bond vectors comprising the SiOSi angles. With one exception, they are also coordinated by larger banana-shaped isosurfaces oriented perpendicular to the plane centered in the vicinity of the apex of each angle. The hemispherical isosurfaces, ascribed to domains of localized bond-pair electrons, are centered ~0.70 Å along the bond vectors from the oxide anions and the banana-shaped isosurfaces, ascribed to domains of localized nonbonding lone-pair electrons, are centered ~0.60 Å from the apex of the angle. The oxide anion comprising the straight SiOSi angle in coesite is the one exception in that the banana-shaped isosurface is missing; however, it is coordinated by two hemispherically shaped isosurfaces that lie along the bond vectors. In the case of a first-principles model structure generated for stishovite, the oxide anion is coordinated by five hemispherically shaped η-isosurfaces, one located along each of the three SiO bond vectors (ascribed to domains of bonding-electron pairs) that are linked to the anion with the remaining two (ascribed to domains of nonbonding-electron pairs) located on opposite sides of the plane defined by three vectors, each isosurface at a distance of ~0.5 Å from the anion. The distribution of the five isosurfaces is in a one-to-one correspondence with the distribution of the maxima displayed by experimental $\Delta\rho$ and theoretical $-\nabla^2\rho$ maps. Isosurface η maps calculated for quartz and the $(HO)_3SiOSi(OH)_3$ molecule also exhibit maxima that correspond with the $(3,-3)$ maxima displayed by distributions of $-\nabla^2\rho$. Deformation maps observed for the SiOSi bridges for the silica polymorphs and a number of silicates are similar to that calculated for the molecule but, for the majority, the maxima ascribed to lone-pair features are absent. The domains of localized nonbonding-electron pair coordinating the oxide anions of quartz and coesite provide a basis for explaining the flexibility and the wide range of the SiOSi angles exhibited by the silica polymorphs with four-coordinate Si. They also provide a basis for explaining why the SiO bond length in coesite decreases with increasing angle. As found in studies of the interactions of solute molecules with a solvent, a mapping of η-isosurfaces for geometry-optimized silicates is expected to become a powerful tool for deducing potential sites of electrophilic attack and reactivity for Earth materials. The positions of the features ascribed to the lone pairs in coesite correspond with the positions of the H atoms recently reported for an H- doped coesite crystal.

Keywords Deformation · Laplacian and localized electron-density distribution · Quartz · Coesite · Stishovite · Bonding and lone-pair electrons · Sites of potential electrophilic attack

G. V. Gibbs (✉)
Department of Geological Sciences,
Virginia Tech, Blacksburg,
Virginia 24061, USA
e-mail: ggibbs@vt.edu
Fax: + 1-540-231-3386

D. F. Cox
Department of Chemical Engineering, Virginia Tech,
Blacksburg, Virginia 24061, USA

T. D. Crawford
Department of Chemistry, Virginia Tech,
Blacksburg, Virginia 24061, USA

M. B. Boisen Jr
Department of Mathematics,
University of Idaho,
Moscow, Idaho 83844, USA

M. Lim
Department of Geological Sciences, Virginia Tech,
Blacksburg, Virginia 24061, USA

Introduction

Electron-density distributions, ρ, observed and calculated for the silica polymorphs and representative silicic acid molecules, have been studied with a variety of strategies with the aim of improving our understanding of the SiO-bonded interactions and establishing a connection between localized and locally concentrated features of the electron density, chemical behavior, structural properties, and sites of potential chemical reactivity and attack. These strategies include a mapping of the deformation $\Delta\rho$ electron-density distribution, the Laplacian $-\nabla^2\rho$ distribution and the electron localization function, η. The features displayed by these distributions will be compared and related to those of the valence-shell electron pair repulsion (VSEPR) model (Gillespie 1970) and to the positions of the H atoms recently reported for an H-doped coesite crystal synthesized at high pressures and temperatures (Koch-Müller et al. 2001).

Deformation electron-density distributions

The deformation electron-density distribution is defined to be the difference between the actual electron-density distribution and an independent atom model (IAM) electron-density distribution that consists of spherically averaged, static ground-state atoms placed at the positions that they occupy in the unit cell V of a crystal. Such a distribution, generated with the expression

$$\Delta\rho(\mathbf{r}) = 1/V \sum_{hkl} [|F_{\mathrm{obs}}(\mathbf{r}^*)|/k - |F_{\mathrm{IAM}}(\mathbf{r}^*)|] \times \exp(-2\pi\mathbf{r}\cdot\mathbf{r}^* + i\alpha) \ ,$$

displays how the observed electron-density distribution of the bonded array of atoms differs from an IAM distribution, where $\mathbf{r} = x\mathbf{a} + y\mathbf{b} + z\mathbf{c}$ and $\mathbf{r}^* = h\mathbf{a}^* + k\mathbf{b}^* + l\mathbf{c}^* \cdot |F_{\mathrm{obs}}(\mathbf{r}^*)|$ are the observed structural amplitudes determined from experimental X-ray diffraction intensity data and $|F_{\mathrm{IAM}}(\mathbf{r}^*)|$ are the structural amplitudes calculated for the IAM model where each amplitude is phased in terms of the model by the phaser $\exp(i\alpha)$. In addition, each $|F_{\mathrm{obs}}(\mathbf{r}^*)|$ is scaled by the factor k determined in the least-squares refinement of the crystal structure.

In the case of the silica polymorphs, $\Delta\rho$ maps have been successful in delineating domains of accumulation (maxima) of electron density along SiO bond vectors connecting adjacent Si and O atoms ascribed to bond-pair electrons, but have had little success in delineating domains that can be ascribed to nonbonding-electron pairs. For example, each of the experimental $\Delta\rho$ maps, generated with sets of single-crystal X-ray diffraction data recorded for the silica polymorphs quartz (Stewart et al. 1980) coesite (Geisinger et al. 1980; Downs 1995), and stishovite (Hill et al. 1983; Spackman et al. 1987; Kirfel et al. 2001) displays maxima in the vicinity of the SiO bond vectors. These maxima are typically offset from the vectors toward the interior of the SiOSi angle and toward the more electronegative oxide anions. For the majority of the maps, few or no other maxima of significance are displayed (Stewart et al. 1980; Hill et al. 1983; Geisinger et al. 1987; Spackman et al. 1987). Two exceptions are maps recorded for the O5 oxide anion of the $Si_1O_5Si_2$ angle in coesite and the anion in stishovite.

The O5 anion in coesite, in addition to being coordinated by maxima along the Si_1O_5 and Si_2O_5 bond vectors, is coordinated by a third maximum that is centred in the vicinity of the apex of the $Si_1O_5Si_2$ angle on the reflex side of the angle (Fig. 1; Geisinger et al. 1980; Downs 1995). Based on a simple hybridization model of the atomic orbitals centered on the anion, Downs (1995) suggested that the distribution of the three maxima is consistent with the formation of sp^2 rather than sp^3 hybrid domains ascribed to one nonbonding-electron pair and two bonding-electron pair regions of localized electron density. In contrast, for stishovite, where each oxide anion is bonded in a plane to three Si cations, maxima occur not only in the vicinity of each of the SiO bond vectors, but also on opposite sides of the plane directly above and below the anion (Spackman et al. 1987). Unlike the silica polymorphs with a four-coordinate Si and a two-coordinate oxide anion, the maxima in stishovite are offset from two equivalent SiO bond vectors (comprising the shared edges between adjacent SiO_6 octahedra) toward the exterior of the OSiO and SiOSi angles with a maximum lying along a third bond vector to the anion. Although they were observed to occur in the vicinity of the bond vectors in the three polymorphs, their heights were

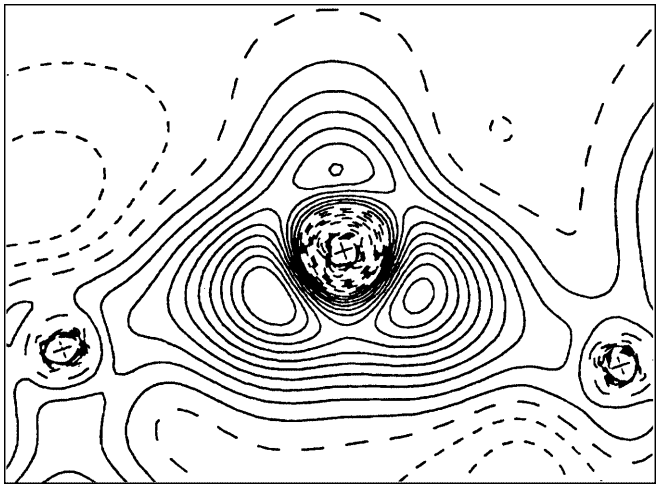

Fig. 1 Experimental static model deformation electron-density $\Delta\rho$ map for the $Si_1O_5Si_2$ plane in coesite. The contour interval is 0.05 e Å^{-3}. The *long-dashed line* represents the zero level contour, the *short-dashed lines* represent the negative level line contours and the *solid line* contours represent the positive level line contours. The O5 oxide anion is located at the + *at the center of the map*, Si_1 is located at the + *at the left* and Si_2 is located at the + *at the right of the anion*

found to be largely independent of the observed SiO bond lengths. A more recent mapping of the deformation electron-density distribution, based on accurate synchrotron diffraction data (Kirfel et al. 2001), has yielded maps that are similar to those recorded by Spackman et al. (1987). It was also found that the heights of the maxima along the SiO bonds are independent of the lengths of the SiO bonds (Kirfel et al. 2001).

In contrast, the observed SiO bond lengths of coesite decrease in a regular way with increasing SiOSi angle (Gibbs et al. 1977) in agreement with a Mulliken population analysis that yields bond overlap populations that increase with decreasing bond length and increasing SiOSi angle (Gibbs et al. 1977; Newton and Gibbs 1980). Further, the value of the electron density evaluated at the bond-critical points has since been found to increase in a regular way with decreasing bond length (Gibbs et al. 2000). Despite these trends, the heights of the maxima along the SiO bonds displayed in the $\Delta\rho$ maps were found to be independent of the observed SiO bond lengths as reported for stishovite (Geisinger et al. 1980; Downs 1995). Deformation maps calculated for a number of silicic acid molecules were also found to display well-defined maxima along each of the SiO bond vectors with maxima located next to the bridging oxide anions bisecting the SiOSi angle (Geisinger et al. 1980) as observed for the $Si_1O_5Si_2$ angle in coesite. The maxima in the calculated maps were found to be offset from the SiO bond vectors toward the interior of the SiOSi angle and toward the oxide anions as observed for the silica polymorphs. Also, the heights of the maxima displayed by the calculated maps tend to be smaller than those observed and to decrease with decreasing bond length. A deformation map, calculated in a perpendicular plane bisecting the SiOSi angle of the $(HO)_3SiOSi(OH)_3$ molecule, was found to display an elongated flat- topped ridge of electron density rather than two maxima that bisect the angle as predicted by the VSEPR theory. A static deformation map for the SiOSi angle of the monosilicate chain in spodumene was recently generated in a relatively accurate high-resolution Ag$K\alpha$ X-ray diffraction experiment (Kuntzinger and Ghermani 1999). The map is topologically similar to that observed for the $Si_1O_5Si_2$ plane in coesite and that calculated for $(HO)_3SiOSi(OH)_3$ molecule. It is not clear from the evidence provided for spodumene whether the feature that bisects the SiOSi angle comprises an elongate flat-topped ridge or a pair of maxima.

In a review of the $\Delta\rho$ electron density distributions and the SiO-bonded interactions for more than 20 silicates, including the silica polymorphs, Tsirelson et al. (1990) concluded, on the basis of the accumulation of the electron density in maxima along the bond vectors and at the interior of the SiOSi angle, that the bond is predominately covalent, with a substantial component of double-bond character. In sharp contrast, on the basis of similar evidence, Cohen (1994) concluded that the bond is highly ionic with nearly fully ionized Si cations and oxide anions. Gillespie and Johnson (1997) reached a similar conclusion in a study of the bond-critical point properties of the calculated electron-density distribution for the $H_3SiOSiH_3$ molecule. Also, Gavie et al. (2000) concluded, on the basis of projected local densities for the orbital valence states of Si and O atoms, that the SiO bond is markedly ionic in quartz. However, on the basis of the high compressibilities of quartz and cristobalite, the observed accumulation of electron density ($\sim$1.0 e Å^{-3} in the regions of the SiO bond-critical points and the failure of an ionic model to reproduce the structures and elastic properties, Gibbs et al. (1999) concluded that the SiO-bonded interaction is more intermediate in character than asserted by these workers (see also Gibbs et al. 2000).

Little or no effort was made in the study of the deformation maps to establish a link between features that can be ascribed to localized domains of bonding and particularly nonbonding electrons and the maxima displayed by the $\Delta\rho$ maps (Tsirelson et al. 1990). In addition to Downs' (1995) suggestion of nonbonding- and bonding-pair domains on the O5 anion in coesite, Spackman et al. (1987) argued that the maxima located above and below the oxide anion is stishovite can likewise be ascribed to localized domains of nonbonding electrons. In this case, however, three bonding domains are arranged in a plane like an sp^2 hybrid orbital with a single lone-pair domain oriented perpendicular to the plane of the hybrid orbitals. However, despite similar deformation maps observed for stishovite, Kirfel et al. (2001) concluded that the accumulation of electron density ascribed to the domain of nonbonding electrons by Spackman et al. (1987) is an artifact caused by systematic errors in the observational diffraction dataset rather than a feature that can be ascribed to nonbonded interactions.

Local charge concentration of the valence electron-density distributions

A mapping of $-\nabla^2\rho(\mathbf{r})$, where $\nabla^2\rho(\mathbf{r}) = \partial^2\rho(\mathbf{r})/\partial x^2 + \partial^2\rho(\mathbf{r})/\partial y^2 + \partial^2\rho(\mathbf{r})/\partial z^2$, highlights those domains where the electron-density distribution of a bonded array of atoms is locally concentrated, resulting in the formation of $(3,-3)$ maxima. As demonstrated by Bader et al. (1984), Bader and MacDougall (1985), MacDougall (1989), and Bader (1990), these maxima bear a close connection with the distribution of the bonding and nonbonding electron-pair domains associated with representative Lewis electron pairs (1966) assumed in the VSEPR model of molecular structure.

A mapping of the $-\nabla^2\rho$ distribution for the geometry-optimized structures, generated for quartz and the $(HO)_3SiOSi(OH)_3$ molecule, revealed three maxima associated with the bridging oxide anion, ascribed to one nonbonding- and to two bonding-pair electron domains of locally concentrated electron density.

Despite the fact that the number of atoms in a quartz crystal far exceeds that of the molecule, the sizes, positions, and shapes of the maxima in both materials are similar, a result that suggests that the electron-density distributions of the two are governed in large part by similar forcefields (Gibbs et al. 2001). However, the number of maxima displayed by the anion is at odds with the number displayed by the $-\nabla^2\rho$ distribution of the anion in a variety of other oxide materials, i.e., the water molecule (Bader et al. 1984). Unlike quartz, for example, the distribution for the oxide anion of the molecule displays four maxima ascribed to two nonbonding- and two bonding-electron domains of locally concentrated electrons, as predicted by Lewis' (1966) valence theory and the VSEPR model for the molecule (Gillespie and Hargittai 1997). However, like the oxide anion of water, each of the nonbridging oxide anions of the $(HO)_3SiOSi(OH)_3$ molecule displays four maxima, the larger two ascribed to domains of nonbonding-electron pairs and the smaller two to bonding-electron pairs along the SiO and OH bonds. This result is consistent with the VSEPR theory, which assumes that domains of nonbonding electrons are more space-filling than domains of bonding electrons and can exert a greater repulsive force on other domains of paired electrons. It should be noted in passing that the oxide anion in a molecule like CSO also displays a single nonbonding-electron pair domain, as observed for quartz (Bader 1990).

In an assessment of the overall shape of the region of local concentration of ρ for the SiOSi bridge, a three-dimensional representation of the $-\nabla^2\rho$ distribution was generated for the $(HO)_3SiOSi(OH)_3$ molecule (Gibbs et al. 2001). The innermost and outermost spherical envelopes of the distribution displayed in Fig. 2 define zero-level isosurfaces where ρ is neither locally concentrated nor locally depleted. Enclosed between these envelopes, there exists a single, highly elongated crescent-shaped set of isosurfaces that are disposed in the plane that bisects the SiOSi angle centered ~0.35 Å from the apex of the angle. The concentric isosurfaces, centered on a maximum value of 25 e $Å^{-5}$, wrap about half way around the anion. The region between the zero-level isosurface is where the electron density distribution is locally concentrated. As such, this feature can be ascribed to a single, crescent-shaped nonbonding-electron domain of locally concentrated electron density. In contrast, a three-dimensional representation of the $-\nabla^2\rho$ distribution for the oxide anion of the water molecule displays two separate sets of crescent-shaped isosurfaces displayed in a plane that bisects the HOH angle centered 0.37 Å from the apex of the angle (Gibbs et al. 2001). However, as observed for the OH bonds of the water molecule, a 3-D representation of the $-\nabla^2\rho$ distribution cut along the plane of the SiOSi angle of the $(HO)_3SiOSi(OH)_3$ molecule revealed a set of crescent-shaped isosurfaces along each of the SiO bonds. The sizes of the domains defined by these isosurfaces are substantially smaller than those

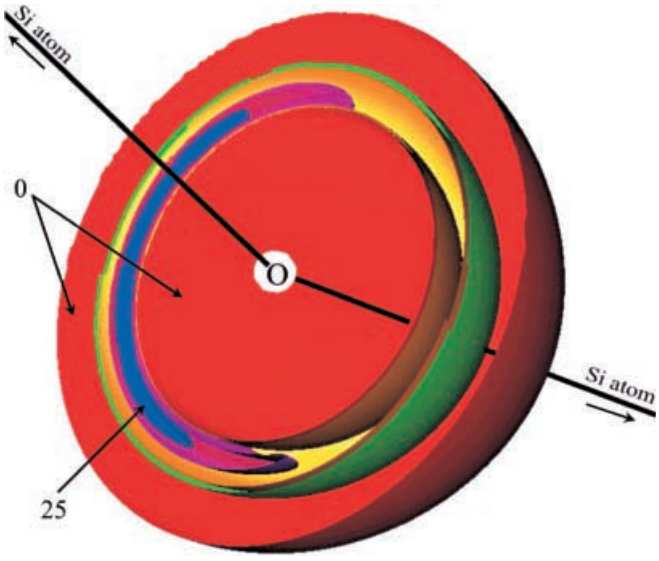

Fig. 2 A three-dimensional representation of the valence shell charge concentration (VSCC) isosurfaces calculated for the bridging oxide anion of the $(OH)_3SiOSi(OH)_3$ molecule cut in a perpendicular plane bisecting the SiOSi angle. The *white sphere at the center* of the figure represents the oxide anion and the *heavy lines radiating from the anion* represent the SiO bond vectors. The *innermost* and *outermost red envelopes* represent zero isosurfaces where the electron density is neither locally concentrated nor locally depleted. The features of the figure indicate that the electron density is progressively more locally concentrated from the red isosurfaces toward the blue elongate crescent-shaped isosurface where the VSCC adopts a maximum value of ~25 e $Å^{-5}$. This feature can be ascribed to a single domain of nonbonding electrons centered at a distance of 0.35 Å directly above the oxide anion

ascribed to the nonbonding local concentrations for corresponding values of the Laplacian. It is notable that a deformation map (Fig. 3), calculated along a perpendicular plane that bisects the HOH angle of the water molecule, also displays two well-defined maxima at a distance of 0.2 Å from the oxide anion, 0.1 Å closer to the anion than the corresponding maxima displayed by the $-\nabla^2\rho$ distribution. Also, the lpOlp angle displayed by the $\Delta\rho$ map is ~160°, 20° wider than that displayed by the $-\nabla^2\rho$ distribution. Nonetheless, despite the different strategies, both maps display a qualitatively similar distribution of maxima.

Electron localization function

As the electron localization function (Becke and Edgecombe 1990) has been used with considerable success in highlighting regions of electron localization in molecules and crystals (cf. Savin et al. 1997; Burdett and McCormick 1998; Trout and Parrinello 1999; Chesnut 2000; Fuster et al. 2000), the function was evaluated for the geometry-optimized crystal structures of quartz, coesite, and stishovite (Gibbs et al. 1999, 2000) as well as for chemically and structurally related geometry-optimized molecules for purposes of comparing the calculated features with those displayed in $\Delta\rho$ and $-\nabla^2\rho$ maps. It is

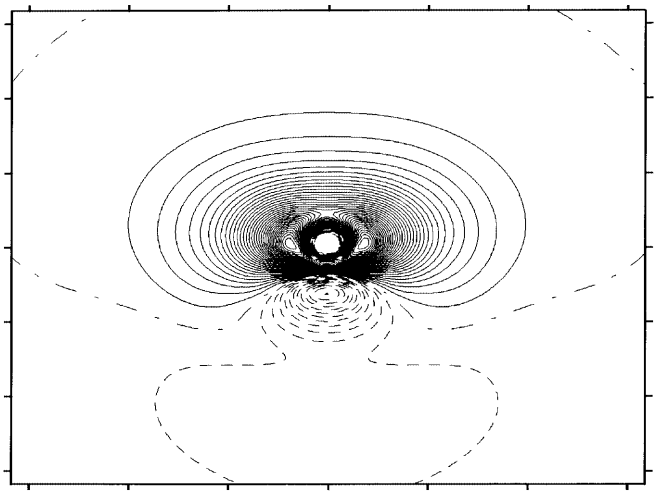

Fig. 3 Deformation map for the water molecule calculated for a perpendicular plane bisecting the HOH angle. The geometry of the molecule was optimized at the B3LYP 6-311G(2d,p) level. The *level line contours* are drawn at a 0.05 e Å^{-3} interval, the *solid lines* denote positive contours, the *dashed lines* denote negative contours and the *dash-dot line* denotes the zero level contour

anticipated that isosurfaces of the ELF function will aid our effort to explain the structural relationships and properties of the polymorphs in terms of the localization of the electrons. It will also aid in linking the $(3,-3)$ maxima displayed in $-\nabla^2\rho$ maps to maxima displayed in $\Delta\rho$ maps ascribed to domains of nonbonding electrons. As domains of bonding and nonbonding electrons have played a pivotal role in the rationalization of the structures, properties, and reactivity of molecules, it is also anticipated that they will play a similar role in the study of the silica polymorphs (Bader 1990). In a recent polarized IR spectroscopic examination of an H-doped coesite crystal, Koch-Mueller et al. (2001) found that the H atoms are bonded only to the oxide anions O2, O3, O4, and O5, but not to O1. To satisfy the local charge imbalance, they suggested that a vacant site that houses an Si_2 cation in the crystal is surrounded by four OH groups. It will be of interest to see whether the domains of electron localization ascribed to domains of nonbonding electrons (sites of potential electrophilic attack by the protons, for example) in coesite serve to differentiate the properties of O1 from those of the remaining oxide anions and provide a basis for explaining why H avoids O1 yet has an affinity for the O2, O3, O4, and O5 anions.

The electron localization function, $\eta(\mathbf{r})$, as defined by Becke and Edgecombe (1990), is given by the expression

$$\eta(\mathbf{r}) = \left(\frac{1}{1+\chi^2(\mathbf{r})}\right) \quad , \tag{1}$$

where

$$\chi(\mathbf{r}) = \frac{\left(\sum_i |\nabla\psi(\mathbf{r})_{i,\sigma}|^2 - \frac{1}{8}|\nabla\rho(\mathbf{r})_\sigma|^2/\rho(\mathbf{r})_\sigma\right)}{0.3483 \times \rho(\mathbf{r})_\sigma^{5/3}} \quad , \tag{2}$$

$\rho(\mathbf{r})_\sigma = \sum_i |\psi(\mathbf{r})_{i,\sigma}|^2$ is the one-electron density evaluated at $\mathbf{r}$ where i runs over all one electron σ-spin orbitals, $\psi(\mathbf{r})_{i,\sigma}$, and $\rho(\mathbf{r})_\sigma^{5/3}$ is the kinetic energy density of a homogeneous electron gas with spin density equal to the local value of $\rho(\mathbf{r})_\sigma$ likewise evaluated at $\mathbf{r}$ (Becke and Edgecombe 1990; Savin et al. 1992). The first term inside the parentheses of Eq. (2) corresponds to the actual electronic kinetic energy density at $\mathbf{r}$, while the second is proportional to the Weizäcker functional which gives the kinetic energy density at $\mathbf{r}$, in a noninteracting-electron approximation. The combination of these two terms is taken to be a measure of the excess kinetic energy due to the Pauli exclusion principle (Fuster et al. 1999). As given, the value of η is restricted to range between 0.0 and 1.0, equaling 0.5 for a homogeneous electron gas. Inasmuch as the Pauli principle has a relatively small impact on the behavior of electrons with antiparallel spins, it can be concluded that the value of the excess local kinetic energy is necessarily relatively small in value and η is relatively large in regions harboring bonding and nonbonding electron-pair domains (regions where electrons with antiparallel spins are localized). In contrast, as the excess local kinetic energy is large in regions where electrons with parallel spins reside, the electrons tend to be delocalized in these regions and η is small, particularly since electrons with parallel spins tend to repel one another by about one order of magnitude greater than those with antiparallel spins (Savin et al. 1997). As such, the electrons of a bonded system tend to be localized into disjoint domains of antiparallel spins as determined by the bonded interactions of a system (Gillespie and Hargittai 1991). In a comparison of the properties of $-\nabla^2\rho$ and η distributions for molecules covering a wide spectrum of bonded interactions, Bader et al. (1998) established a nexus between the domains of electron localization of the η model and domains of local concentration of ρ of the $-\nabla^2\rho$ model to the extent that they can often be topologically related in terms of their numbers and spatial distributions.

In a contrasting study, Burdett and McCormick (1998) pointed out a fundamental problem with the interpretation of the electron localization function in terms of the spin properties of the electrons and Fermi holes. In particular, as reported by Savin et al. (1997), η distributions generated for systems with Hartree-Fock calculations (a method that differentiates between electrons with different spins) often do not differ substantially from those obtained with extended Hückel calculations, a method that utterly fails to distinguish between the spin states of the electrons. Thus, Burdett and McCormick (1998) concluded that there must be another way of interpreting the meaning of the function other than one based on the spin properties of the electrons. In evaluating Eq. (2), they pointed out that the first term inside the parentheses is typically much larger than the second for the majority of molecular and crystalline materials. As such, it was concluded that the ratio $\sum_i |\nabla\psi(\mathbf{r})_{i,\sigma}|^2/\rho(\mathbf{r})_\sigma^{5/3}$ can be considered to be the dominant term in determining the value of η

when evaluated at **r**. Accordingly, large values of the kinetic energy density coupled with small values of $\rho(\mathbf{r})_{\sigma}^{5/3}$ would necessarily result in large values for $\chi(\mathbf{r})$, and vice versa. Since larger contributions to the kinetic energy density generally occur in regions with a higher density of nodes for the occupied orbitals, χ is expected to be large and η is expected to be small in regions where the electrons are delocalized. On the other hand, χ is expected to be small and η large in regions where electrons are localized and where there are few or no nodes to override the contribution of ρ to the value of η at **r** (Burdett and McCormick 1998). If true, then the maxima in the η maps for the silica polymorphs should show a close correspondence with the accumulations of the electron density displayed by the experimental deformation maps. Further, given the correspondence established between the domains of localized and the local concentrated electron-density distribution (Bader 1996), it will be of interest to see whether η and $-\nabla^2\rho$ mappings of the distributions for the silica polymorphs and related molecules yield topologically similar pictures, as reported by Bader et al. (1996).

Character of bonded interactions and the electron localization function

As noted above for a variety of molecular and crystalline materials, η adopts a larger value in those regions where nodal planes are nonexistent and the electron density is localized, and a smaller one in those regions where there are a number of nodal planes and the electron density is delocalized. As such, Savin et al. (1997) have argued that the function is capable of generating "easily understandable pictures of the chemical bond" to the extent that it can be used to provide a basis for establishing the character of a given bonded interaction in terms of the localization of the electron density. Based on earlier work by Kutzelnigg (1984), they asserted at the outset that a closed-shell ionic bonded interaction embodying fully charged cations and anions does not exist. Instead, only intermediate bonded interactions exist, ranging in character between a predominately ionic and shared-electron covalent bonded interactions. According to their arguments, the anions in a predominately ionic material are typically enclosed by a nearly spherical isosurface of a high localization of electron density with a characteristic absence of any localization of electron density along the bond vector connecting the pair of bonded atoms. With increasing covalent character, features ascribed to bonding and nonbonding domains of electron localization materialize and become progressively better developed as the localized bonding domain migrates along the bond pathway from the vicinity of the anion to the center of the bond in an ideal covalent case like, for example, the CC shared electron-bonded interaction in diamond. Accordingly, bonded interactions can be classified on the basis of the position of the localized bonding domain along the bond path; the closer the position of the domain to the midpoint of the path, the greater the shared-electron covalent bonded interaction.

A mapping of η isosurfaces for the silica polymorphs and related molecules

As the pattern of the maxima displayed by the $-\nabla^2\rho$ distribution for the bridging oxide anions of the $(HO)_3SiOSi(OH)_3$ molecule and quartz is similar, η isosurfaces were calculated for the two for purposes of comparison. The calculations of the $\eta(\mathbf{r})$ function were completed using the VASP (Vienna ab-initio simulation package) density functional code (Kresse and Hafner 1993, 1994; Kresse and Furthmüller 1996a, b). Figure 4 displays the 3-D representation of the η isosurface for the molecule calculated with $\eta = 0.844$. The bridging oxide anion, O_{br}, for the molecule is coordinated by a banana-shaped isosurface and two substantially smaller hemispherically shaped isosurfaces. The banana-shaped isosurface is centered at a distance of $\sim$0.60 Å from the apex of the SiOSi angle and wraps part way around the anion, with its long dimension disposed in a plane perpendicular to the angle. The hemispherically shaped isosurfaces are all located about $\sim$0.70 Å along the SiO_{br} bond from the oxide anion. In addition to an ellipsoidal isosurface about the H ion and a hemispherical isosurface along the SiO_{nbr} bond, each of the nonbridging oxide anions, O_{nbr}, is likewise coordinated by a banana-shaped isosurface. It is noteworthy that the isosurface associated with each O_{nbr} is substantially larger than that associated with O_{br}. The hemispherical isosurfaces between the Si atoms and each of the O atoms lie directly along the SiO bond vectors, in contrast with the offset of the maxima from the bonds displayed in the deformation maps. As expected, each of the H cations, which lack core attractors, is enclosed by an ellipsoidally shaped isosurface. The observation that the banana-shaped isosurface about O_{nbr} is substantially larger than that about O_{br} suggests that an O_{nbr} anion will be more susceptible to electrophilic attack than an O_{br} anion.

As observed above, the 3-D representation of the $-\nabla^2\rho$ distribution for the bridging oxide anion of the $(HO)_3SiOSi(OH)_3$ molecule displays a single, highly elongated crescent-shaped envelope of concentric isosurfaces, indicating a single elongated region of locally concentrated electron density. A similar flat-topped ridge is displayed in a mapping of $\Delta\rho$ for the molecule. When the η value for the isosurface of the molecule was increased to $\sim$0.87, the corresponding banana-shaped isosurface of the molecule appeared to disappear as a single entity, showing no evidence of splitting into two separate isosurfaces. Thus, the crescent-shaped feature displayed by the $-\nabla^2\rho$ distribution and the banana-shaped isosurface displayed by η both indicate that the feature ascribed to the domain of nonbonded electrons is localized in a single domain rather than two well-defined

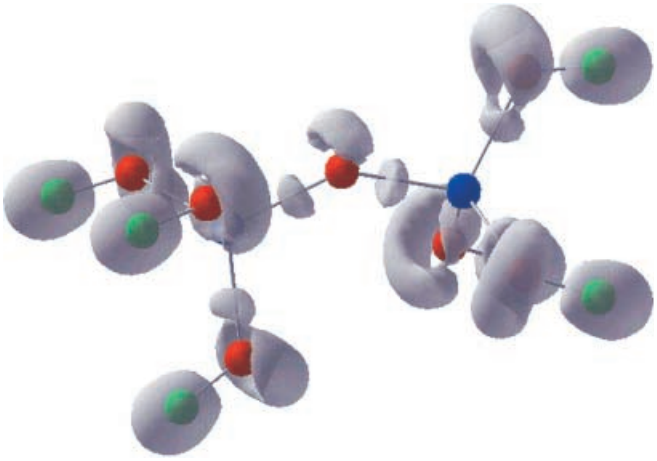

Fig. 4 A three-dimensional η isosurface evaluated for the valence electrons of the $(OH)_3SiOSi(OH)_3$ molecule at an η value of 0.844. The bridging oxide anion is coordinated by two semispherically shaped isosurfaces along the SiO bond vectors ~0.7 Å from the oxide anion and a single banana-shaped isosurface centered ~0.6 Å from the apex of the SiOSi angle. In contrast, each nonbridging oxide anion is coordinated by a semispherical isosurface and a banana-shaped isosurface. A core attractor surrounds the nucleus of each H atom. When the η value was progressively increased in value, the banana-shaped isosurface of the bridging oxide anion remains intact and disappeared as a single unit, whereas that of the nonbridging anion separates into two separate units prior to their disappearance. The *red spheres* represent the oxide anions, the *blue spheres* represent the Si cations and the *green spheres* represent H

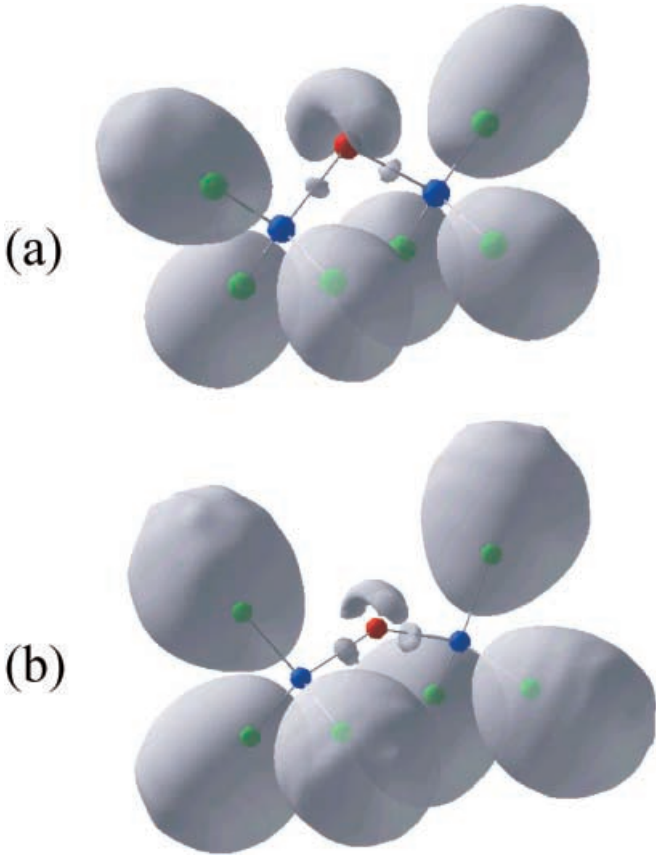

Fig. 5a, b Three-dimensional η isosurfaces evaluated for the valence electrons of the H_3COCH_3 (**a**) and the $H_3SiOSiH_3$ (**b**) molecules evaluated at an η value of 0.844. When the η value is increased in value, the banana-shaped isosurface on the bridging oxide anion of the H_3COCH_3 molecule splits into two well-defined isosurfaces, whereas that of the bridging anion of the $H_3SiOSiH_3$ molecule disappears as a single isosurface. The *red spheres* represent the oxide anions, the *blue spheres* represent carbon in (**a**) and Si in (**b**), and the *green spheres* represent H

domains, as reported for the water molecule (Trout and Parrinello 1999). In contrast, with increasing η values, each of the banana-shaped domains associated with the nonbridging oxide anions, which are bonded to one Si and one H atom, splits into two domains. If the hemispherical isosurfaces together with the banana-shaped isosurface can be ascribed to localized domains of bonding and nonbonding electron pairs, respectively, then it follows that the valence electrons of the bridging oxide anion are localized into three domains, whereas those on the nonbridging oxide anion are localized into four.

A 3-D representation of an η isosurface published for the COC bridge of the methyl acetate molecule likewise displays a relatively large banana-shaped isosurface on the O_{br} anion, oriented perpendicular to the COC plane together with a much smaller hemispherically shaped isosurface displayed about half way along each of the CO_{br} bond vectors (Savin et al. 1997). For purposes of comparison, 3-D representations of η isosurfaces were generated in this study for the two molecules H_3COCH_3 (Fig. 5a) and $H_3SiOSiH_3$ (Fig. 5b). Each displays relatively large banana-shaped isosurfaces located in the vicinity of the bridging angle together with substantially smaller hemispherically shaped isosurfaces along the CO and SiO bridging bond vectors. The banana-shaped feature displayed by the H_3COCH_3 molecule is substantially larger than that displayed by the $H_3SiOSiH_3$ molecule. In contrast, the hemispherically shaped features along the SiO bond vectors of the $H_3SiOSiH_3$ molecule are slightly larger than those along the CO bonds of the H_3COCH_3 molecule. When the value of η for the H_3COCH_3 molecule was progressively increased in value, the banana-shaped isosurface progressively decreases in size and splits into two separate well-defined hemispherical isosurfaces prior to vanishing. In contrast, when the η value is increased for the $H_3SiOSiH_3$ molecule, the banana-shaped isosurface likewise decreases in size and appeared to vanish as a single well-defined entity at an η value of 0.861.

For purposes of comparison, $\Delta\rho$ maps were calculated for the H_3COCH_3 and $H_3SiOSiH_3$ molecules along planes both parallel (Fig. 6) and perpendicular (Fig. 7) to the bridging angle to learn the extent to which the features of the maps correspond with the features displayed by the η and $-\nabla^2\rho$ maps. For the calculations, the geometries of the molecules were both optimized at the B3LYP 6-311G(2d,p) level, assuming C_{2v} point symmetry. The maxima along the CO bond vectors are ~0.28 e Å $^{-3}$ in height and are located halfway along the bond vector (Fig. 6a). The location matches that of

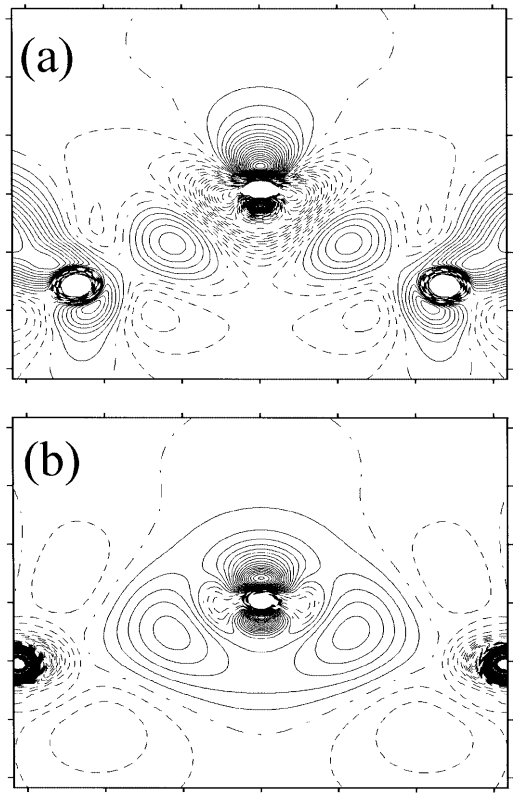

Fig. 6a, b Deformation maps calculated in the plane of the COC angle for the H_3COCH_3 molecule (**a**) and the SiOSi angle of the $H_3SiOSiH_3$ molecule (**b**). The wave functions used to calculate the electron-density distributions were obtained in calculations completed at the BLYP 6-311G(2d,p) level and the promolecule electron-density distributions were generated with the software *SPEEDEN* (R.T. Downs, personal communication). With the output from these two calculations, the deformation maps were calculated with the software DEFORM. The *contour interval* is 0.05 e $Å^{-3}$, the *dashed level lines* represent negative contours, the *solid level lines* represent positive contour and the *dash-dot level line* represents the zero level line

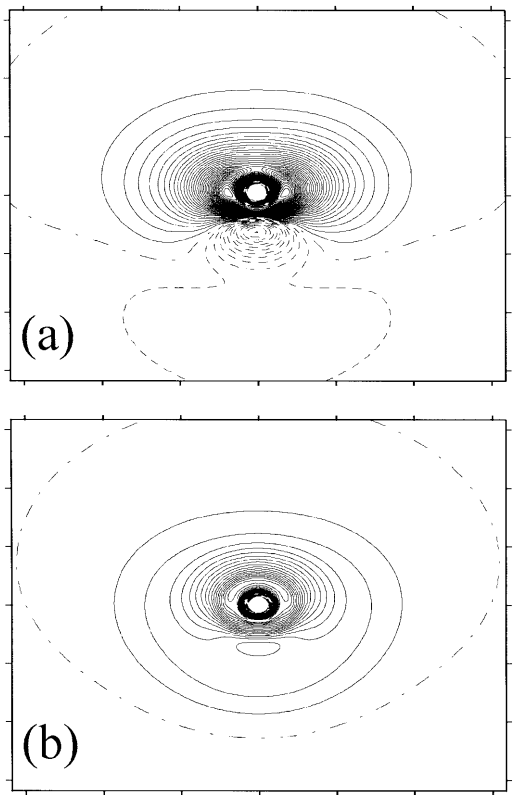

Fig. 7a, b Deformation maps calculated in perpendicular planes that bisect the COC angle for the H_3COCH_3 molecule (**a**) and the SiOSi angle of the $H_3SiOSiH_3$ molecule (**b**). See the legend to Fig. 6 for contour interval information

the isosurfaces displayed along the bond vectors of the η map (Fig. 5a). The maxima along the SiO bond vectors are also $\sim$0.28 e $Å^{-3}$ in height but, unlike the map calculated for the H_3COCH_3 molecule, the 0.1 e $Å^{-3}$ level line contour extends into the interior of the SiOSi angle, enveloping the two maxima along the bond vectors (Fig. 6b). Thus, ρ is localized not only with a maximum along each SiO bond vectors 0.60 Å from the oxide anion, but also in a domain on the interior of the SiOSi angle that connects the two maxima. It is this latter feature, displayed in several observed $\Delta\rho$ maps, that led to the conclusion that the SiO bond exhibits double-bond character (Tsirelson et al. 1990). The deformation maps evaluated in a perpendicular plane (Fig. 7) also display maxima that can be ascribed to domains of nonbonding electron pairs. In the case of the H_3COCH_3 molecule, the distribution exhibits two well-defined maxima located $\sim$0.15 Å from O_{br} (Fig. 7a) while, in the case of the $H_3SiOSiH_3$ molecule, the distribution displays an elongated flat-topped ridge next to the apex of the SiOSi angle that wraps about halfway about O_{br} at a distance of 0.25 Å (Fig. 7b). A close examination of the map revealed that small maxima exist near the ends of the ridge that rise above the flat surface $\sim$0.004 e $Å^{-3}$. A close examination of the flat-topped ridge exhibited by $\Delta\rho$ maps calculated for the $(HO)_3SiOSi(OH)_3$ molecule failed to show such maxima. In addition, the maxima along the bond vectors of the H_3COCH_3 and $H_3SiOSiH_3$ molecules are similar to those displayed by the η maps, whereas the positions of the maxima ascribed to domains of nonbonding electrons are similar to those displayed by the $-\nabla^2\rho$ maps. Indeed, the position along the bond vectors where ρ is indicated to be locally concentrated in the $-\nabla^2\rho$ maps is a region where ρ is indicated to be depleted by the $\Delta\rho$ map. However, it does not necessarily follow that ρ is localized in regions where $-\nabla^2\rho$ is positive and ρ is locally concentrated (Gibbs et al. 2001).

Discussion

As the bond-critical point properties of the silica polymorphs quartz and coesite are similar to those calculated for representative molecules (Gibbs et al. 1999, 2000), 3-D representations of $\eta = 0.844$ isosurfaces for both silica polymorphs were calculated to learn the extent to

which they agree with those calculated for the molecules. The sizes, shapes, and positions of the isosurfaces calculated for the silicate tetrahedron in quartz, displayed in Fig. 8, are strikingly similar to those calculated for the $(HO)_3SiOSi(OH)_3$ and $H_3SiOSiH_3$ molecules. As observed for the bridging oxide anion of these molecules, each oxide anion in quartz is coordinated by a banana-shaped isosurface and two smaller hemispherically shaped isosurfaces displayed along the two nonequivalent SiO bonds. As observed for the molecules, when the η value is increased, the banana-shaped isosurfaces appear to remain intact and to vanish as a single entity.

Unlike quartz, which has one nonequivalent SiOSi angle and two nonequivalent SiO bond lengths, coesite has five nonequivalent SiOSi angles and eight nonequivalent SiO bond lengths. Because of the greater complexity of the coesite structure, it is difficult to depict the isosurfaces of the individual silicate tetrahedra without encountering excessive overlap of the atoms and the isosurfaces that obscures the view. As it was much simpler to depict isosurfaces for the five SiOSi bridges separately, $\eta = 0.844$ isosurfaces were calculated for each of the nonequivalent bridging oxide anions in the structure (Fig. 9). With the exception of the O1 oxide anion, which is involved in a 180° SiOSi angle, each anion is coordinated by a banana-shaped isosurface and two smaller hemispherically shaped isosurfaces. Again, the banana-shaped isosurface appears to vanish as a single unit when the η value is increased. The absence of a banana-shaped feature on the O1 oxide anion suggests that the electron density of the anion is localized primarily along the bond path. This would provide an explanation for why the SiO_1 bonds involved in the 180° angle are the shortest bonds in the structure (Gillespie and Hargittai 1991).

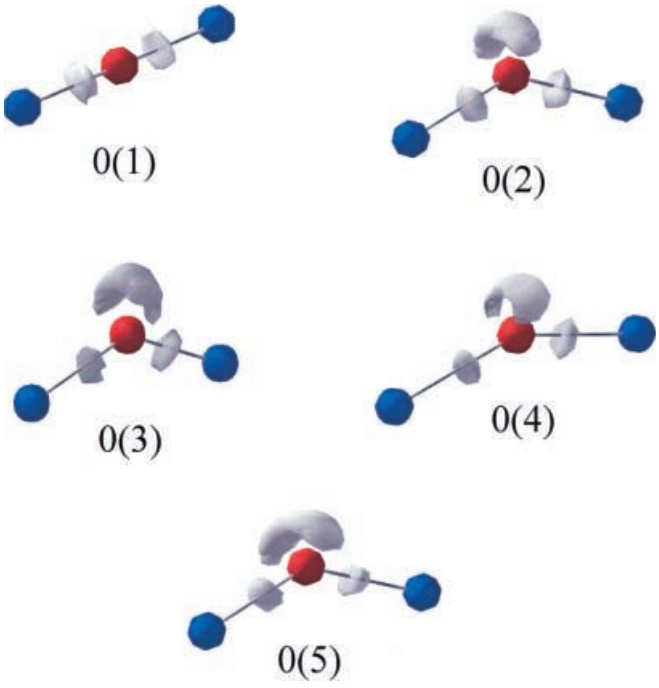

Fig. 9 Three-dimensional representations of η isosurfaces evaluated for the valence electron of the five nonequivalent SiOSi dimers in coesite at an η value of 0.844; the *blue spheres* represent the Si cations and the *red spheres* represent the oxide anions. The O2, O3, O4, and O5 oxide anions are involved in bent SiOSi angles and display two hemispherical isosurfaces along each SiO bond at a distance of ~0.7 Å from the oxide anion and a banana-shaped surface centered ~0.06 Å from the apex of the SiOSi angle oriented perpendicular to the angle. The O1 anion involves a straight SiOSi and displays hemispherical isosurfaces along the SiO bond vectors. Each of the surfaces was evaluated at an η value of 0.844

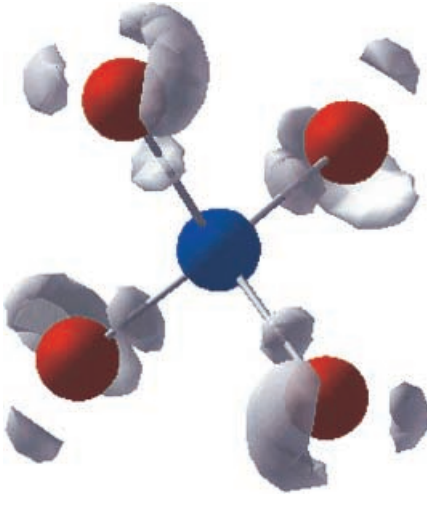

Fig. 8 A three-dimensional representation of the η surfaces evaluated for the valence electrons for the silicate tetrahedral oxyanion in quartz evaluated at an η value of 0.844. The *central blue sphere* represents Si and the *four red spheres* represent the oxide anions. Each oxide anion is coordinated by two hemispherical isosurfaces along the SiO bond vectors ~0.7 Å from the oxide anion and a banana-shaped surface centered ~0.6 Å from the apex of the SiOSi angle oriented perpendicular to the angle. The SiO bonds from the oxide anions to the next nearest Si cations are not displayed, but the hemispherical isosurfaces along these bonds are displayed

Clearly, the η maps show that the valence-shell features of O1 are substantially different from those of O2, O3, O4, and O5. The latter oxide anions are all endowed with a feature that can be ascribed to a domain of nonbonding electrons, whereas O1 lacks this feature. As such, O2, O3, O4, and O5 are sites of potential electrophilic attack by H, whereas H is expected to avoid O1. Subsequent to our calculations, we learned that Koch-Müller et al. (2001) had located the positions of the protons in an H-doped coesite crystal, using spectroscopic methods. Our results predict that the protons would avoid O1 and attack and bond to the O2, O3, O4, and O5 anions, a prediction that is in exact agreement with their spectroscopic analysis.

We are at a loss to explain why the bridging oxide anions of the $(HO)_3SiOSi(OH)_3$ molecule and those involved in the bent SiOSi angles of quartz and coesite all display a feature that can be ascribed to a single localized domain of nonbonding electrons, while each of the bridging anions of the H_2O, $H_3SiOSiH_3$ and the H_3COCH_3 molecules and the nonbridging anions of the

$(HO)_3SiOSi(OH)_3$ molecule displays a feature that can be ascribed to two. Since only three domains of localized electron-density coordinate the bridging oxide anion of an SiOSi bridge, according to the VSEPR model, the constraints imposed on the stereochemistry of the bridge by electron-pair repulsions will be less restrictive than if an additional domain of electron pairs was present. Hence, the SiOSi angles in the silica polymorphs can be expected to be much more compliant and wider than the COC angle, for example. Also, the wide range of angles observed for the polymorphs (135–180°; Gibbs 1982; Navrotsky 1994; Gibbs et al. 1998, 2001) is expected, with the SiOSi angle being much more flexible than the COC angle of a CO_2 framework structure, given that the repulsions among the three domains of localized electrons associated with the SiOSi angle would be much less confining on the geometry that the four domains associated with the COC angle. In a study of the $H_3SiOSiH_3$ molecule, Gillespie and Johnson (1997) observed that the SiO bond is "unusually short" in terms of the Shoemaker-Stevenson rule (1941). They attributed the short bond to a delocalization of the nonbonding-electron density into the vicinity between the Si and O atoms (Gillespie and Hargattai 1991) consistent with the supposition that the strong repulsions between the electron pairs on the oxide anion cause delocalization of these electrons into the partly vacant shell of the silicon atom. It this is true and the electron density is delocalized from the nonbonded region of the oxide anion into the bonding region (Figs. 1 and 6b), then this would not only provide a mechanism for explaining why the banana-shaped domain of localized electron density is relatively small and disappears as a single entity with an increase in the η value, but world also explain why the SiOSi angle is observed to be very compliant and why the SiO bond length decreases with increasing angle (Gibbs 1982; Gibbs et al. 2001).

As observed above, unlike the bulk of the silica polymorphs, which consist of silicate tetrahedral oxyanions, each Si atom in stishovite is bonded to six oxide anions disposed at the corner of an octahedron and each O atom is bonded to three Si atoms at the corners of a triangle. The atoms in a unit cell of the stishovite structure are displayed in Fig. 10 together with an η map evaluated at $\eta = 0.844$. The map displays five hemispherically shaped isosurfaces about the oxide anions, three along the SiO bond vectors, and one above and one below the oxide anion. In effect, the distribution of the isosurfaces in the η distribution is in a one-to-one correspondence with distribution of maxima in the observed deformation maps (Spackman et al. 1987). Thus, if the $\eta(\mathbf{r})$ function highlights domains where electrons are localized, as argued by Burdett and McCormick (1998), then it would appear that deformation maps recorded for the silica polymorphs highlight similar features. The presence of the hemispherical η isosurfaces above and below the plane of the three SiO bonds is consistent with the Spackman et al. (1987) interpretation of corresponding maxima in the deformation maps as a domain of nonbonded electrons rather than an artifact caused by a poor set of diffraction data (Kirfel et al. 2001). A recent determination of the $(3,-3)$ critical points in a $-\nabla^2\rho$ distribution generated for stishovite displays bonding-electron pair maxima along each of its SiO bonds vectors and nonbonding-electron pair maxima located above and below the oxide anion, as observed by Spackman et al. (1987) and displayed in the η map (Fig. 10). Thus, in the case of the silica polymorphs, the overall features of the $\Delta\rho$, $-\nabla^2\rho$, and η distributions are topologically similar, with their maxima in a one-to-one correspondence. Thus, it appears that each of the three strategies yields information about similar properties of the electron-density distribution.

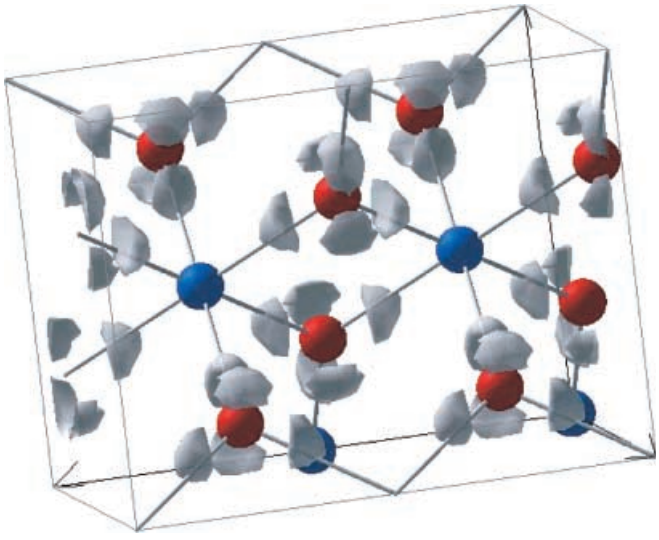

Fig. 10 A drawing of the structure of stishovite. Each Si cation (represented by a *blue sphere*) is bonded to six oxide anions (represented by a *red spheres*) and each oxide anion is bonded to three Si cations. Each oxide anion is coordinate by five hemispherical η isosurfaces evaluated for the valence electrons at an η value of 0.844. The isosurfaces along the SiO bond vectors that comprise the shared edges of the SiO_6 octahedra are displaced from the bond vectors to the exterior of the OSiO angles, whereas that of the remaining one lies along the SiO bond. The remaining two isosurfaces are located above and below the oxide anion along a line oriented perpendicular to the three Si cations that coordinate the oxide anion. The surface was evaluated at an η value of 0.844

Concluding remarks

The features displayed by $-\nabla^2\rho$ and η distributions generated for model structures of the silica polymorphs, related silicates, and representative molecules are topologically similar to those displayed by several calculated and experimental $\Delta\rho$ distributions. However, the positions of the maxima along the bond vectors displayed by $-\nabla^2\rho$ maps are much closer to oxide anions than those displayed by the η and $\Delta\rho$ maps. In contrast, maxima ascribed to nonbonding domains are substantially closer to the anion in the $-\nabla^2\rho$ and $\Delta\rho$ maps. If the maxima in

$-\nabla^2\rho$ and η distributions are signatures of domains of bonding and nonbonding electrons, then the maxima displayed by representative deformation maps can likewise be considered to be signatures of these electrons (Koritsanszky and Coppens 2001). The presence of localized domains in the electron-density distribution for the silica polymorphs, silica glass, and silicates provides a basis for the relatively large variation in the SiOSi angle and the large variety of structure types adopted by silicates. Just as the determination of regions of local concentration and localization of electron-density distributions for molecules can be used as a sound basis for deducing sites of potential electrophilic attack by an incoming substituent (Bader et al. 1985; MacDougall 1989; Fuster er al. 2000), it follows that regions in a silicate where the electron density is greater than an AIM distribution provide similar information. The strikingly similar $-\nabla^2\rho$ and η distributions displayed by the silica polymorphs and representative molecules indicated that the forces that govern the electron-density distributions behave as if short-ranged and molecular-like (Gibbs et al. 2001).

Hemispherically shaped η isosurfaces occur $\sim$40% of the way along the SiO bond vectors from the oxide anion in quartz, coesite, and the $H_3SiOSiH_3$ and $(HO)_3SiOSi(OH)_3$ molecules, in support of Pauling's (1960) assertion from electronegativity consideration that the bond is intermediate in character (Gibbs et al. 1999). As the isosurfaces are located $\sim$35% of the way along the SiO bond vectors in stishovite, the bonded interactions comprising the SiO_6 octahedra in stishovite are indicated to be somewhat more ionic than those comprising silicate tetrahedral. Clearly, the arguments that the SiO bond is a closed-shell ionic bonded interaction involving Si^{4+} and O^{2-} ions is not supported by the theoretical and observed electron-density distributions (Gibbs et al. 2001).

Acknowledgements G.V.G. and M.B.B. are grateful to the National Science Foundation for supporting this work with grant EAR-9627458; D.F.C. gratefully acknowledges financial support by the Chemical Sciences, Geosciences, and Biosciences Division, Office of Basic Energy Sciences, Office of Science, US Department of Energy through grant DE-FG02-97ER14751; and T.D.C. wishes to thank the Camille and Henry Dreyfus Foundation for the New Facility Award, which supported his contribution to this work. M.L. wishes to thank the Research Division at Virginia Tech for supporting his visit to the University with a Research Fellowship. The bulk of this paper was written while G.V.G. was a National Science Foundation Funded Visiting Scholar at the University of Arizona during the spring of 2001. The faculty and graduate students of the Department of Geosciences, and Bob Downs and George Lager in particular, are thanked for making the visit great fun and a productive experience. Professor Donald Chesnut of the Chemistry Department at Duke University is thanked for his helpful comments on the meaning of the electron localization function, and Jim Downs is thanked for providing a deformation map for the $Si_1O_5Si_2$ plane in coesite. We also wish to thank the two reviewers for making a number of helpful suggestions that clearly improved the manuscript. We also thank Dr. Koch-Müller for supplying us with an early version of her paper on the determination of the proton positions in H-doped coesite.

References

Bader RFW (1990) Atoms in molecules. Oxford Science Publications, Oxford, UK

Bader RFW, MacDougall PJ (1985) Toward a theory of chemical reactivity based on charge density. J Am Chem Soc 107: 6788–6795

Bader RFW, MacDougall PJ, Lau CDH (1984) Bonded and nonbonded charge concentrations and their relation to molecular geometry and reactivity. J Am Chem Soc 106: 1594–1605

Bader RFW, Johnson S, Tang TH, Popelier PLA (1996) The electron pair. J Phys Chem (A) 100: 15398–15415

Becke AD, Edgecombe KE (1990) A simple measure of electron localization in atomic and molecular systems. J Chem Phys 92: 5397–5403

Burdett JK, McCormick TA (1998) Electron localization in molecules and solids: the meaning of ELF. J Phys Chem (A) 102: 6366–6372

Chesnut DB (2000) The electron localization function signature of the amide bond exhibits nitrogen lone-pair character. J Phys Chem (A) 104: 7635–7638

Cohen RE (1994) First-principle theory of crystalline silica, SILICA. Reviews in mineralogy, vol. 29, Chap 10, Heaney PJ, Prewitt CT, Gibbs GV (eds) Am Mineral Washington, DC 369–402

Downs JW (1995) The electron-density distribution of coesite. J Phys Chem 99: 6849–6856

Fuster F, Sevin A, Silvi B (2000) Topological analysis of the electron localization function (ELF) applied to electrophile aromatic substitution. J Phys Chem (A) 104: 852–858

Geisinger KL, Spackman MA, Gibbs GV (1987) Exploration of structure, electron-density distribution and bonding in coesite with Fourier and pseudoatom refinement methods using single crystal X-ray diffraction data. J Phys Chem 91: 3237–3244

Gibbs GV (1982) Molecules as models for bonding in silicates. Am Mineral 67: 421–450

Gibbs GV, Prewitt CT, Baldwin KJ (1977) A study of the structural chemistry of coesite. Z Kristallogr 145: 108–123

Gibbs GV, Spackman MA, Boisen MB (1992) Bonded and promolecule radii for crystals and molecules. Am Mineral 77: 741–750

Gibbs GV, Boisen MB, Hill FC, Tamada O (1998) SiO- and GeO-bonded interactions as inferred from the bond-critical point properties of electron-density distributions. Phys Chem Miner 25: 674–584

Gibbs GV, Rosso KM, Teter DM, Boisen MB, Bukowinski MST (1999) Model structures and properties of the electron density distribution for low quartz at pressure: a study of the SiO bond. J Mol Struct 485–486: 13–25

Gibbs GV, Boisen MB, Rosso KM, Teter DM, Bukowinski MST (2000) Model structures and electron density distributions of the silica polymorph coesite at pressure: an assessment of OO-bonded interactions. J Phys Chem (B) 104: 10534–10542

Gibbs GV, Boisen MB, Beverly LL, Rosso KM (2001) A computational quantum-chemical study of the bonded interactions in Earth materials and structurally and chemically related molecules, Molecular modeling theory: applications in the geosciences. Reviews in Mineralogy and Geochemistry, vol. 42, Cygan RT, Kubicki JD (eds) Rosso JJ (series ed) Mineralogical Society of America, Washington, DC 345–382

Gillespie RJ (1970) The valence-shell electron pair model of molecular geometry. J Chem Educ 4718–4723

Gillespie RJ, Hargittai I (1991) The VSEPR model of molecular geometry. Allyn and Bacon, Boston, Massachussetts 1–248

Gillespie RJ, Johnson SA (1997) Study of bond angles and bond lengths in disiloxane and related molecules in terms of the topology of the electron density and its Laplacian. Inorg Chem 36: 3031–3039

Hill RJ, Newton MD, Gibbs GV (1983) A crystal-chemical study of stishovite. J Solid State Chem 47: 185–200

Kirfel A, Krane HG, Blaha P, Schwartz K, Lippmann T (2001) Electron-density distribution in stishovite, SiO_2: a high-energy synchrotron radiation study. Acta Crystallogr (A) 57: 663–677

Koch-Müller M, Fei Y, Hauri E, Liu Z (2001) Location and quantitative analysis of OH in coesite. Phys Chem Miner 28: 693–705

Koritsanszky TS, Coppens P (2001) Chemical applications of X-ray charge density analysis. Chem Rev 101: 1583–1627

Kresse G, Furthmüller J (1996a) Efficiency of ab initio total energy calculations for metals and semiconductors using a plane-wave basis set. Comput Mat Sci 6: 15–50

Kresse G, Furthmüller J (1996b) Efficient iterative schemes for ab initio total-energy calculations using a plane-wave basis set. Phys Rev (B) 54: 11169–11186

Kresse G, Hafner J (1993) Ab initio molecular dynamics for liquid metals. Phys Rev (B) 47: 558–561

Kresse G, Hafner J (1994) Ab initio molecular-dynamics simulation of the liquid-metal amorphous-semiconductor transition in germanium. Phys Rev (B) 49: 14251–14269

Kuntzinger S, Ghermani NE (1999) Electron density and Madelung potential in α-spodumene, $LiAl(SiO_3)_2$, from two-wavelength high-resolution X-ray diffraction data. Acta Crystallogr (B) 55: 273–284

Kutzelnigg W (1984) Chemical bonding in higher main group elements. Ang Chem Inter Ed English, 23: 272–295

Lewis GN (1966) Valence and the structure of atoms and molecules. Dover Press, New York, NY

MacDougall PJ (1989) The Laplacian of the electron charge distribution. PhD Thesis, McMaster University 1–128

Navrotsky A (1994) Thermochemistry of crystalline and amorphous silica, SILICA. Reviews in Mineralogy, vol. 29, Chap 9, Heaney PJ, Prewitt CT, Gibbs GV (eds) American Mineralogist, Washington, DC 307–329

Newton MD, Gibbs GV (1980) Ab initio calculated geometries and charge distributions for H_4SiO_4 and $(OH)_3SiOSi(OH)_3$ compared with experimental values for silicates and siloxanes. Phys Chem Miner 6: 221–246

Pauling L (1960) The nature of the chemical bond, 3rd ed. Cornell University Press, Ithaca, NY

Savin A, Nesper R, Wengert S, Fässler TF (1997) ELF: the electron localization function. Ang Chem Inter Ed English, 36: 1808–1832

Shoemaker V, Stevenson DP (1941) Some revisions of the covalent radii and the additivity rule for the lengths of partially ionic single covalent bonds. J Am Chem Soc 63: 37–40

Spackman MA, Hill RJ, Gibbs GV (1987) Exploration of structure and bonding in stishovite with Fourier and pseudoatom. Phys Chem Miner 14: 139–150

Stewart RP, Whitehead WA, Donnay G (1980) The ionicity of the SiO bond in low quartz. Am Mineral 65: 324–326

Trout BL, Parrinello M (1999) Analysis of the dissolution of H_2O using first-principles molecular dynamics. J Phys Chem (B) 103: 7340–7345

Tsirelson VG, Evdokimova OA, Belokoneva EL, Urusov VS (1990) Electron-density distribution and bonding in silicates: a review of recent data. Phys Chem Miner 17: 275–292